AMSE Association for the Advancement of Modelling & Simulation Techniques in Enterprises
IIETA International Information and Engineering Technology Association
Advancing the World of Information and Engineering

Advances in Modelling and Analysis C
Vol. 73, No. 2, June, 2018, pp. 29-36
Journal homepage:http://iieta.org/Journals/AMA/AMA_C

Comparative study between luenberger observer and extended kalman filter for fault-tolerant control of induction motor drives

Toufik Roubache[1,2*], Souad Chaouch[2], Mohamed S. Naït-Saïd[2]

[1] Electrical Engineering Dep., Msila 28000, Algeria
[2] LSP-IE, Electrical Engineering Dep., Batna 2 05078, Algeria

Corresponding Author Email: toufik.roubache@gmail.com

Received: March 3 2018
Accepted: May 22 2018

Keywords:
active fault tolerant control (AFTC), input-output linearization controls (IOLC), induction motor drives (IMD), luenberger observer (LO), extended kalman filter (EKF), electric vehicle (EV)

ABSTRACT

In this paper, a robust active fault tolerant control (AFTC) scheme is proposed for induction motor drives (IMD) via input-output linearization control (IOLC) and nonlinear observer. In order to estimate the states and to reconstruct the faults, two different observers are used; a Luenberger observer (LO) and an extended kalman filter (EKF). Further we introduce feedback linearization strategy by choosing the output function as the rotor speed and flux square. To provide a direct comparison between these FTCs schemes, the performance is evaluated using the control of IMD under failures, variable speed, and variable parameters, finally the obtained results show that the proposed controller with the proposed observers provides a good trajectory tracking, and these schemes are robust with respect to faults, parameter variations, and external load disturbances for induction motor drive system.

1. INTRODUCTION

Induction motor (IM), in particular, squirrel cage IM is crucial in industries for many reasons, such as simple construction, low maintenance requirement, rigid and high reliability like compressors [1-3]. Recent developments in many modern technologies have offered an excellent opportunity to use AC motors in high performance drives systems. Induction motor is attracting attention in recent years and it is widely recognized to be a very suitable candidate for hybrid and electric vehicles (EVs) applications. Robustness, high starting torque, cruising speed and high controllability are some of the IM characteristics responsible for its wide utilization in traction applications such as electric vehicles (EVs) [4-6].

Many industrial applications require high dynamic performances and robustness to different perturbations. Thus, the robust control algorithm is desirable in stabilization and tracking trajectories.

Fault-Tolerant Control Systems (FTCS) can be classified into two types: passive (PFTCS) and active (AFTCS). In this paper, we are concerned with the design and analysis of active FTCs. Contrasting with the former, the latter react with system component failures actively and implement reconfiguring actions to maintain the system stable and with acceptable performance [2]. The robust nonlinear FTCs considered here use the input-output feedback linearization control, based on differential geometry techniques. These techniques allow us to decompose the model of the motor in two independent mono-variable linear sub-systems. The dynamics of each sub-system is obtained by an optimal pole placement [6]. In addition, input-output linearization control can offer a good insensitivity to parameters variations, external disturbances and rejection faults [7-9]. Fault-tolerant control schemes are characterized in this work by their capabilities, after fault occurrence, to recover performance close to the nominal desired performance. In addition, their ability to react successfully (stably) during a transient period between the fault occurrence and the performance recovery is an important feature.

In this paper, we propose exploring the AFTC concept in EV propulsion by developing two architectures applied to an induction-motor drive affected by a sensor fault and used nonlinear controls via input-output feedback linearization. The first architecture is an AFTC include a Luennberger observer (FTC-LO). The second architecture is the combined between FTC and an Extended kalman filter (FTC-EKF). Our objective is to design an active fault-tolerant controller to maintain the stability, robustness and tracking performance of the faulty system. The main contributions of the paper are as follows: Firstly, two sensorless controls are considered in the paper, which is more practical in the control engineering. Secondly, an application of the FTCs techniques, especially with a holistic view on the electric vehicles (EVs). This later becomes very attractive in replacing conventional internal combustion engine vehicles because of environmental and energy issues. In addition EVs are by many seen as the cars of the future as they are high efficient, produces no local pollution, are silent, and can be used for power regulation by the grid operator [11-14]. The comparison between AFTC of induction motor based on LO and EKF schemes ensures the validity of the proposed technique.

This paper is organized as follows. In section 2, a model of IM under faults and EV dynamics are introduced. Section 3 reviews an attitude control technique using input-output linearization controls (IOLC). A sensorless control based on nonlinear observers is discussed in Section 4. The proposed fault tolerant control is explained in section 5. In Section 6 numerical simulation and a qualitative comparative study between these two FTCs structures are carried out to evaluate the performance of the robust FTCs. Finally, in section 7 concluding remarks are stated.

2. MODELING OF IM UNDER FAULTS AND EV DYNAMICS

2.1 Induction motor with faulty model

The standard mathematical faulty model of the IM in stationary frame is given by [15]:

$$\dot{x} = F + Gu + \gamma f_s \tag{1}$$

where f_s *i*s the actuator fault, γ and G are constants matrix, F is a nonlinear matrix given by:

$$F = \begin{bmatrix} a_1 i_{s\alpha} + a_2 \varphi_{r\alpha} + a_3 \omega \varphi_{r\beta} \\ a_1 i_{s\beta} - a_3 \omega \varphi_{r\alpha} + a_2 \varphi_{r\beta} \\ a_4 i_{s\alpha} + a_5 \varphi_{r\alpha} - \omega \varphi_{r\beta} \\ a_4 i_{s\beta} + \omega \varphi_{r\alpha} + a_5 \varphi_{r\beta} \end{bmatrix} \tag{2}$$

$$\begin{cases} x = [x_1\ x_2\ x_3\ x_4]^T = \left[i_{s\alpha}\ i_{s\beta}\ \Phi_{r\alpha}\ \Phi_{r\beta}\right]^T \\ G = \begin{bmatrix} g_1 & 0 & 0 & 0 \\ 0 & g_2 & 0 & 0 \end{bmatrix}^T \\ u = [u_1\ \ u_2]^T = [v_{s\alpha}\ \ v_{s\beta}]^T \end{cases} \tag{3}$$

$$\begin{cases} \gamma = \begin{bmatrix} 1 & 0 & 0 & 0 \\ 0 & 1 & 0 & 0 \end{bmatrix}^T \\ f_s = [f_{s1}\ \ f_{s2}]^T \end{cases} \tag{4}$$

For simplicity, we define the following variables:

$$\begin{cases} a_1 = \frac{-R_t}{\sigma L_s}, a_2 = \frac{1-\sigma}{L_m \sigma T_r}, a_3 = \frac{L_m}{L_s \sigma L_r}, a_4 = \frac{L_m}{T_r} \\ a_5 = -\frac{1}{T_r}, a_6 = a_4,\ a_7 = \frac{L_m}{J L_r}, a_8 = -\frac{T_L}{J} \\ g_1 = g_2 = \frac{1}{\sigma L_s} \end{cases} \tag{5}$$

where $\sigma = 1 - \frac{{L_m}^2}{L_s L_r}$ is the coefficient of dispersion, L_s, L_r, L_m are respectively stator, rotor and mutual inductance. R_s, R_r are respectively stator and rotor resistance. T_r is the rotor time constant ($T_r = \frac{L_r}{R_r}$). J, T_L are inertia moment of the moving element and load torque.

The presence of electrical and/or mechanical faults generates asymmetry of the IM yielding some slot harmonics in the stator winding:

$$\begin{cases} i_{s\alpha} \to i_{s\alpha} + F_{hs1} \\ i_{s\beta} \to i_{s\beta} + F_{hs2} \end{cases} \tag{6}$$

where:

$$\begin{cases} F_{hs1} = \sum_i^{f_{s1}} A_i sin(\omega_i t + \varphi_i) \\ F_{hs2} = \sum_i^{f_{s2}} A_i cos(\omega_i t + \varphi_i) \end{cases} \tag{7}$$

In the IM, the presence of faults shows harmonic components on the stator currents with known frequency and unknown amplitude and phase. The frequency dependent on the kind of fault which belongs to the two possible classes (rotor or stator faults), and the amplitude and phase dependent on the fault severity.

Let us the following exosystem [15-16]:

$$\dot{\psi}_f(t) = \lambda_f(\varpi)\psi_f(t), \psi_f \in \Re^{4n_f+2} \tag{8}$$

where $\varpi = \left[\omega_1\ \ \omega_{2,1}\ \ \omega_{2,-1}\ ..\ \omega_{2,n_f}\ \ \omega_{2,-n_f}\right]$ is the vector of the pulsations, and we have:

$$\begin{cases} \lambda_f = diag\left(\lambda_{fi}\right) \\ \lambda_{fi} = \begin{bmatrix} 0 & \omega_1 & 0 & 0 \\ -\omega_1 & 0 & & \\ \vdots & & \ddots & \vdots \\ 0 & & \cdots & 0 \quad \omega_i \\ & & & -\omega_i \quad 0 \end{bmatrix} \\ \psi_f = \begin{bmatrix} \psi_{2i-1} \\ \psi_{2i} \end{bmatrix} \in \Re^{4n_f+2}, i = 1, \dots, n_f \end{cases} \tag{9}$$

where n_f is faults number, and $\omega_i = 2\pi(f_i + f_a)$ is the pulsation under faults.

Then (6) can be expressed as:

$$\begin{cases} i_{s\alpha} \to i_{s\alpha} + \Theta_1 \psi_f \\ i_{s\beta} \to i_{s\beta} + \Theta_2 \psi_f \end{cases} \tag{10}$$

with:

$$\begin{cases} \Theta_1 = [1\ \ 0\ \ 1\ \ 0\ \ ...\ \ 1\ \ 0] \\ \Theta_2 = [0\ \ 1\ \ 0\ \ 1\ \ ...\ \ 0\ \ 1] \end{cases} \tag{11}$$

2.2 Vehicle model

Vehicle dynamics model only concerns the longitudinal dynamics of the vehicle [17]. In this case electric vehicle use independently equipped motors to drive each wheel. The independently equipped motors provide higher power/weight density, higher reliability for safety, and better dynamic performance, the dynamic differential equations for the longitudinal motion of the vehicle can be described as:

$$J_w \frac{d\omega_w}{dt} = (T_m - T_L) \tag{12}$$

$$M_v \frac{dV_v}{dt} = (F_L - F_r) \tag{13}$$

$$V_w = R_w \omega_w \tag{14}$$

$$F_L(\lambda_L) = \mu N \tag{15}$$

$$\lambda_L = \frac{V_w - V_v}{V_w} \tag{16}$$

The vehicle model is based on mechanics and aerodynamics principles [18-19]. The total tractive effort is then given by:

$$F_r = F_{ad} + F_{ro} + F_{pr} + F_{sf} \tag{17}$$

The power required to drive a vehicle, at a speed V_v, has to compensate counteracting forces [11, 20].

$$P_v = V_v F_r = V_v\left(F_{ad} + F_{ro} + F_{pr} + F_{sf}\right) \tag{18}$$

where the definition of all parameters is listed in Table1. Generally, the nonlinear interrelation ships between the slip ratio λ_L and friction coefficient μ_L formed by tire dynamics can be modeled by the widely adopted Magic Formula [21].

Table 1. EV parameters

Parameters	Describe
J_w	Wheel inertia
ω_w	Wheel rotation
T_m	Driving torque
R_w	Wheel radius
T_L	Load torque
M_v	Vehicle mass
V_v	Vehicle velocity
F_L	Friction force (driving force)
F_r	Road load force
λ_L	Slip ratio
μ_L	Friction coefficient
N	Vehicle weight
F_{ad}	Aerodynamic drag force
F_{ro}	Rolling resistance force
F_{pr}	Profile force of the road
F_{sf}	Stokes friction force

A programmable DC machine is utilized to emulate the longitudinal dynamics characteristics of the vehicle and a DC-DC converter, as can be seen in Fig.1. As a mechanical load emulator.

3. INPUT-OUTPUT LINEARIZATION CONTROLLER

The input-output linearization technique uses a nonlinear change of coordinates and feedback to transform the nonlinear system (1) into a decoupled linear one. The design technique is based on generating a direct relationship between the output *y* and the control input *u* and then cancelling the present nonlinearities through the appropriate choice of control inputs. In this section, a similar approach has been applied to rotor speed and rotor flux control of IM drive using the model presented in stationary frame (Eq.1).

In order to create a direct relation between system outputs (*y*) and inputs (*u*), the output variable is chosen by $y_1 = \varphi_r$ and $y_2 = \omega$.

$$y = \begin{bmatrix} y_1 \\ y_2 \end{bmatrix} = \begin{bmatrix} h_1 \\ h_2 \end{bmatrix} = \begin{bmatrix} {\varphi_{r\alpha}}^2 + {\varphi_{r\beta}}^2 = \varphi_r \\ \omega \end{bmatrix} \tag{19}$$

Therefore, the output dynamics could be easily written as follows:

$$y_1 : \begin{cases} \dot{h}_1(x) = L_f h_1(x) = 2a_5 L_m f_1 - 2a_5 \varphi_r \\ \ddot{h}_1(x) = L_f^2\, h_1(x) + L_{G_\alpha} L_f h_1(x) u_{s\alpha} + L_{G_\beta} L_f h_1(x) u_{s\beta} \end{cases} \tag{20}$$

with:

$$\begin{cases} L_f^2\, h_1(x) = 2a_4 a_5 L_m f_3 - (2a_1 a_4 + 6a_4 a_5) f_1 \\ \qquad\qquad +2a_4 \omega f_2 + \left(\frac{4}{T_r} a_5 + 2a_2 a_4\right) \varphi_r \\ L_{G_\alpha} L_f h_1(x) = 2a_2\, L_r \varphi_{r\alpha} \\ L_{G_\beta} L_f h_1(x) = 2a_2\, L_r \varphi_{r\beta} \end{cases} \tag{21}$$

$$y_2 : \begin{cases} \dot{h}_2(x) = L_f h_2(x) = \frac{pL_m}{JL_r} f_2 - \frac{C_r}{J} \\ \ddot{h}_2(x) = L_f^2\, h_2(x) + L_{G_\alpha} L_f h_2(x) u_{s\alpha} + L_{G_\beta} L_f h_2(x) u_{s\beta} \end{cases} \tag{22}$$

with:

$$\begin{cases} L_f^2\, h_2(x) = \frac{pL_m}{JL_r} \omega f_1 - \frac{pL_m}{JL_r}(a_1 + a_5) f_2 - \frac{{pL_m}^2}{{JL_r}^2} \frac{\omega}{\sigma L_s} \varphi_r \\ L_{G_\alpha} L_f h_2(x) = -\frac{pL_m}{JL_r} \frac{1}{\sigma L_s} \varphi_{r\beta} \\ L_{G_\beta} L_f h_2(x) = \frac{pL_m}{JL_r} \frac{1}{\sigma L_s} \varphi_{r\alpha} \end{cases} \tag{23}$$

where: $f_1 = i_{s\alpha}\varphi_{r\alpha} + i_{s\beta}\varphi_{r\beta}$, $f_2 = i_{s\beta}\varphi_{r\alpha} - i_{s\alpha}\varphi_{r\beta}$ $f_3 = {i_{s\alpha}}^2 + {i_{s\beta}}^2$

Although the system dynamics order is five, the output dynamics have the order of four which implies the presence of an internal dynamics and the corresponding stability could be easily proven.

Using input-output feedback linearization, only the derivatives of the outputs are considered, we obtain:

$$\begin{bmatrix} \ddot{h}_1 \\ \ddot{h}_2 \end{bmatrix} = \begin{bmatrix} L_f^2 h_1(x) \\ L_f^2 h_2(x) \end{bmatrix} + \mathrm{E(x)} \begin{bmatrix} u_{s\alpha} \\ u_{s\beta} \end{bmatrix} \tag{24}$$

with:

$$E(x) = \begin{bmatrix} L_{G_\alpha} L_f h_1(x) & L_{G_\beta} L_f h_1(x) \\ L_{G_\alpha} L_f h_2(x) & L_{G_\beta} L_f h_2(x) \end{bmatrix} = \begin{bmatrix} 2a_2 L_r \varphi_{r\alpha} & 2a_2 L_r \varphi_{r\beta} \\ -\frac{pL_m}{JL_r} \frac{1}{\sigma L_s} \varphi_{r\beta} & \frac{pL_m}{JL_r} \frac{1}{\sigma L_s} \varphi_{r\alpha} \end{bmatrix} \tag{25}$$

$$Det\,[E(x)] = 2\frac{a_2 L_r}{\sigma L_s} \varphi_r \tag{26}$$

If $\varphi_r \neq 0$, the matrix $E(x)$ is non-singular. By defining v as the new control input for linear system of:

$$v = \begin{bmatrix} v_1 \\ v_2 \end{bmatrix} = \begin{bmatrix} L_f^2 h_1(x) \\ L_f^2 h_2(x) \end{bmatrix} + \mathrm{E(x)} \begin{bmatrix} u_{s\alpha} \\ u_{s\beta} \end{bmatrix} \tag{27}$$

Main control equation can be defined as:

$$\begin{bmatrix} u_{s\alpha} \\ u_{s\beta} \end{bmatrix} = \mathrm{E(x)}^{-1} \left(\begin{bmatrix} -L_f^2 h_1(x) \\ -L_f^2 h_2(x) \end{bmatrix} + \begin{bmatrix} v_1 \\ v_2 \end{bmatrix} \right) \tag{28}$$

As a result, the system control effort would be simplified to:

$$v_1 = \ddot{h}_1 = \frac{d^2\varphi_r}{dt^2} = k_{\varphi 1}\left(\varphi_{ref} - \varphi_r\right) + k_{\varphi 2}\left(\frac{d\varphi_{ref}}{dt} - \frac{d\varphi_r}{dt}\right) + \frac{d^2\varphi_{ref}}{dt^2} \tag{29}$$

$$v_2 = \ddot{h}_2 = \frac{d^2\omega}{dt^2} = k_{\omega 1}\left(\omega_{ref} - \omega\right) + k_{\omega 2}\left(\frac{d\omega_{ref}}{dt} - \frac{d\omega}{dt}\right) + \frac{d^2\omega_{ref}}{dt^2} \tag{30}$$

The gains $k_{\varphi 1}$, $k_{\varphi 2}$, $k_{\omega 1}$ and $k_{\omega 2}$ are chosen by identification with a second order system by using the pole placement method.

4. SENSORLESS NONLINEAR CONTROL OF INDUCTION MOTOR

4.1 The luenberger observer

The Luenberger observer, estimates states of the system (stator current and rotor flux). The observer equation can be given as:

$$\frac{d\hat{x}}{dt} = A\hat{x} + Bu + K_L(i_s - \hat{i}_s) \tag{31}$$

where K_L is the observer gain matrix which governs the dynamics and the observer's robustness; it is calculated by:

$$K_L = \begin{bmatrix} K_1 & K_2 & K_3 & K_4 \\ K_2 & -K_1 & K_4 & -K_3 \end{bmatrix}^T \tag{32}$$

The coefficients $K_1, K_2, K_3,$ and K_4 are defined as follows [22]:

$$\begin{cases} K_1 = (k-1)\left[\frac{1}{\sigma L_s} + \frac{(1-\sigma)}{\sigma T_r} + \frac{1}{T_r}\right] \\ K_2 = (K-1)\hat{\omega} \\ K_3 = \frac{(1-k^2)}{a_3}\left[\frac{1}{\sigma L_s} + \frac{(1-\sigma)}{\sigma T_r} + \frac{1}{T_r}\right] + \frac{(k-1)}{a_3}\left[\frac{1}{\sigma L_s} \right. \\ \qquad \left. + \frac{(1-\sigma)}{\sigma T_r} + \frac{1}{T_r}\right] \\ K_4 = \frac{(k-1)}{a_3}\hat{\omega}, \ \ k > 0 \end{cases} \tag{33}$$

The estimated speed is obtained from the speed tuning signal by using a PI controller thus:

$$\hat{\omega} = K_p\left(z_1\hat{\varphi}_{r\beta} - z_2\hat{\varphi}_{r\alpha}\right) + K_i\int\left(z_1\hat{\varphi}_{r\beta} - z_2\hat{\varphi}_{r\alpha}\right)dt \tag{34}$$

where $z_1 = \varphi_{r\alpha} - \hat{\varphi}_{r\alpha}$ and $z_2 = \varphi_{r\beta} - \hat{\varphi}_{r\beta}$ are errors between the estimated and measured rotor flux. K_p, K_i are proportional and integral positive gains.

4.2 The extended Kalman filter

The extended Kalman filter is an optimal state estimator for nonlinear dynamical systems. An EKF will be used for the reconstruction of the faults of the induction motor model using current measurements. Since EKF is a stochastic filter, the discrete nonlinear stochastic model of the induction motor must be used and can describe by [23]:

$$\begin{cases} X(k+1) = g[X(k), u(k), k] + b_{rs}(k) \\ Y(k+1) = c_d X(k) + b_{rm}(k) \end{cases} \tag{35}$$

where $Y(k)$ is a vector containing the α - β components of the stator current space vector, $u(k)$ is a vector of excitation signals, which are the α - β components of the stator voltage space vector, $X(k)$ is a vector containing the states, $b_{rs}(k)$ and $b_{rm}(k)$ are respectively the process and the measurement noise vectors at time k. the covariance matrix of noise vector, which is shown below:

$$Q = cov(w) = E\{ww^T\}; R = cov(v) = E\{vv^T\}$$

where Q and R are respectively the process and the measurement covariance matrices. $E\{ww^T\}$ represents the mathematical expectation [24].

The Extended Kalman Filter equations are [23, 25]:

$$\begin{cases} P(k+1\,|k) = F(k)P(k)F(k)^T + Q \\ K(k+1) = P(k+1\,|k)C^T[CP(k+1\,|k)C^T + R]^{-1} \\ \hat{X}(k+1) = g\left[\hat{X}(k), u(k)\right] + K(k)\left[Y(k) - C\hat{X}(k)\right] \end{cases} \tag{36}$$

where $\hat{X}$ is the state estimate, $P(k)$ is the estimation error covariance matrix, $K(k)$ is the Kalman gain matrix, $F(k)$ and C are given by:

$$\begin{cases} F(k) = \frac{\partial}{\partial X}\{g[X(k), u(k), k]\} \\ C = \frac{\partial}{\partial X}\{c_d(X(k), k)\} \end{cases} \tag{37}$$

It can be seen that the structure of EKF is similar to that of LO, except that its gain K is designed to minimize the error between the real and estimated state vectors.

The speed adaptive mechanism is given by:

$$\hat{\omega} = K_p\left(z_1\hat{\varphi}_{r\beta} - z_2 i_{s\beta}\hat{\varphi}_{r\alpha}\right) + K_i\int\left(z_1\hat{\varphi}_{r\beta} - z_2\hat{\varphi}_{r\alpha}\right)dt \tag{38}$$

5. ROBUST FAULT TOLERANT CONTROL

This section proposes an active FTC approach using nonlinear observer and based on nonlinear control in the presence of faults, and only actuator faults are considered in the design procedure as well. the fault tolerant architecture proposed in this paper is illustrated in figure (1). Therefore, in this paper, two active FTC strategies which will be discussed later, are all based on the input-output linearization control for a purpose also to compare the advantages and disadvantages of a FTC strategies based on two nonlinear observers (LO and EKF) with the same fundamental control technique.

5.1 Fault reconstruction

The healthy state of current sensor for phase in the frame (α, β) could be judged from an error variable $e_{s\alpha\beta}$.

$$e_{s\alpha\beta} = |i_{s\alpha} - \hat{\imath}_{s\alpha}| + \left|i_{s\beta} - \hat{\imath}_{s\beta}\right| \tag{39}$$

The dynamics of the estimation error under actuator faults is given by this system:

$$\dot{\tilde{e}}_x = \begin{bmatrix} \dot{x}_1 \\ \dot{x}_2 \end{bmatrix} - \begin{bmatrix} \dot{\hat{x}}_1 \\ \dot{\hat{x}}_2 \end{bmatrix} = \begin{bmatrix} i_{s\alpha} \\ i_{s\beta} \end{bmatrix} - \begin{bmatrix} \dot{\hat{\imath}}_{s\alpha} \\ \dot{\hat{\imath}}_{s\beta} \end{bmatrix} \tag{40}$$

$$\dot{\tilde{e}}_x = 0 \Leftrightarrow \begin{cases} (1-a_1)\tilde{z}_{x1} - \lambda_1 tanhz_{y1} - f_{s1} = 0 \\ (1-a_1)\tilde{z}_{x2} - \lambda_2 tanhz_{y2} - f_{s2} = 0 \end{cases} \tag{41}$$

Equation (41) shows that z_x converges to zero, as $t \to \infty$, $\hat{\imath}_{s\alpha}$ and $\hat{\imath}_{s\beta}$ could be calculated based on the full order observer (LO or EKF) above. Thus, the fault is estimated by the following expression:

$$\begin{cases} \hat{f}_{s1} = -\Gamma_1 tanhz_{y1} \\ \hat{f}_{s2} = -\Gamma_2 tanhz_{y2} \end{cases} \tag{42}$$

The function *tanh* represents a hyperbolic function. Γ_1 and Γ_2 are selected constant vector and $(z_{y1} = y_1 - \hat{y}_1,\ z_{y2} = y_2 - \hat{y}_2)$ are the output estimation errors.

5.2 Control reconfiguration

In the case of global control reconfiguration, $\hat{f}_{s1} \rightarrow f_{s1}$ and $\hat{f}_{s2} \rightarrow f_{s2}$, then the faults are compensated and the resulting additional control laws (u_{1ad} and u_{2ad}) can be expressed by:

$$\begin{cases} u_{1ad} = -\frac{1}{g_1}\hat{f}_{s1} \\ u_{2ad} = -\frac{1}{g_2}\hat{f}_{s2} \end{cases} \quad (43)$$

6. SIMULATION RESULTS

In this section, some numerical simulations have been performed to validate the proposed FTC schemes. The induction motor parameters are given in the appendix.

The closed-loop simulation results are reported in Figures below under both healthy and faulty conditions, and this demonstrates that the disturbance and fault rejection are guaranteed truly.

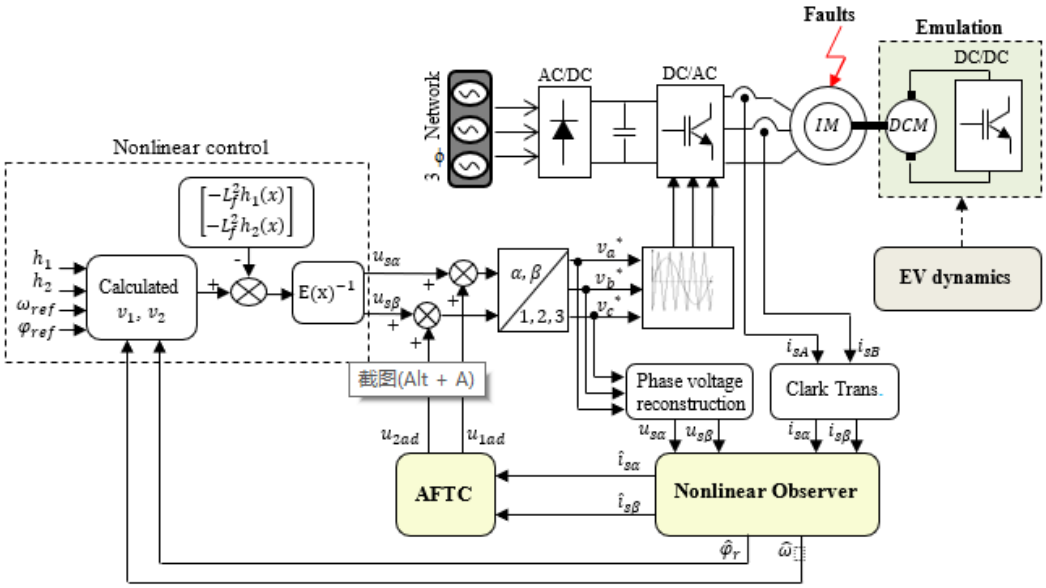

Figure 1. Block diagram of the proposed active fault tolerant control for IMD

In the all simulations cases, for fair comparison the same measurements are assumed available to both deterministic and stochastic observers and the same controller parameters are used.

On the other hand variations of 50% of the stator resistance (R_s) and rotor resistance (R_r) between the time t = 14 s and t = 16 s with variable speed reference are introduced. After the faults occurred at t = 12 s. Two levels of simulation results will be presented here: firstly, Figs (2) and (3) show that the simulation results of FTC based on Luenberger observer (LO-FTC).

Simulation results prove that LO-FTC exhibit strong robustness to motor parameter variations, such as stator resistance and rotor resistance. Secondly, Figs (4) and (5) show the results of FTC scheme based on Extended kalman filter (EKF-FTC). The results are obtained with parametric and speed variations.

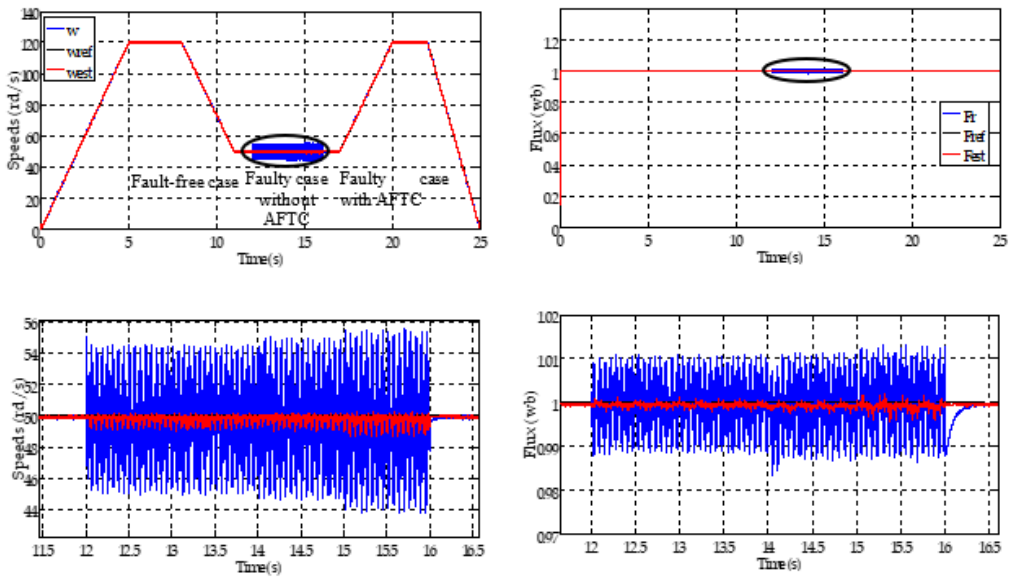

Figure 2. IMD reference, real and estimated speed and rotor flux (upper plot) with using LO-FTC strategy, and zoom around fault appearance at t = 12 s (lower plot)

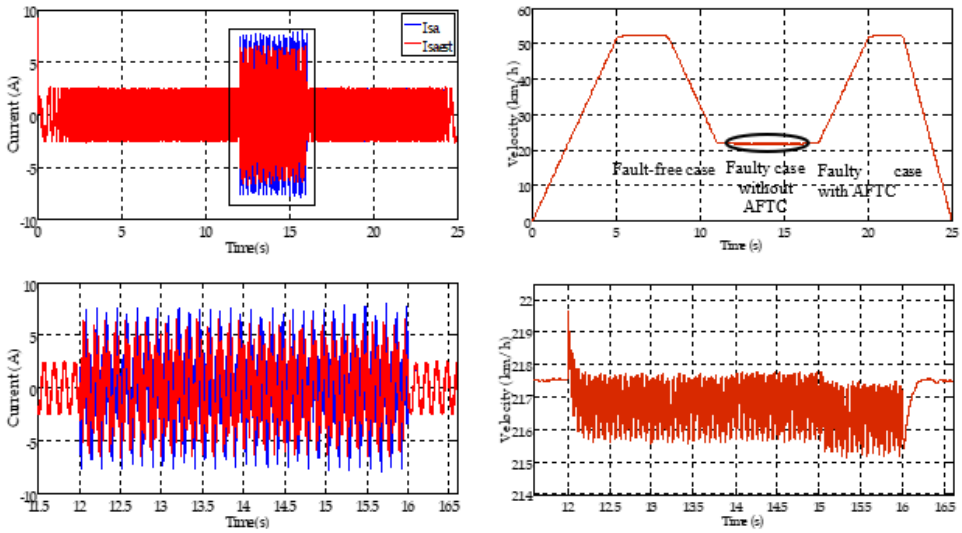

Figure 3. Current and EV velocity (upper plot) with using LO-FTC strategy, and zoom around fault appearance at t = 12 s (lower plot)

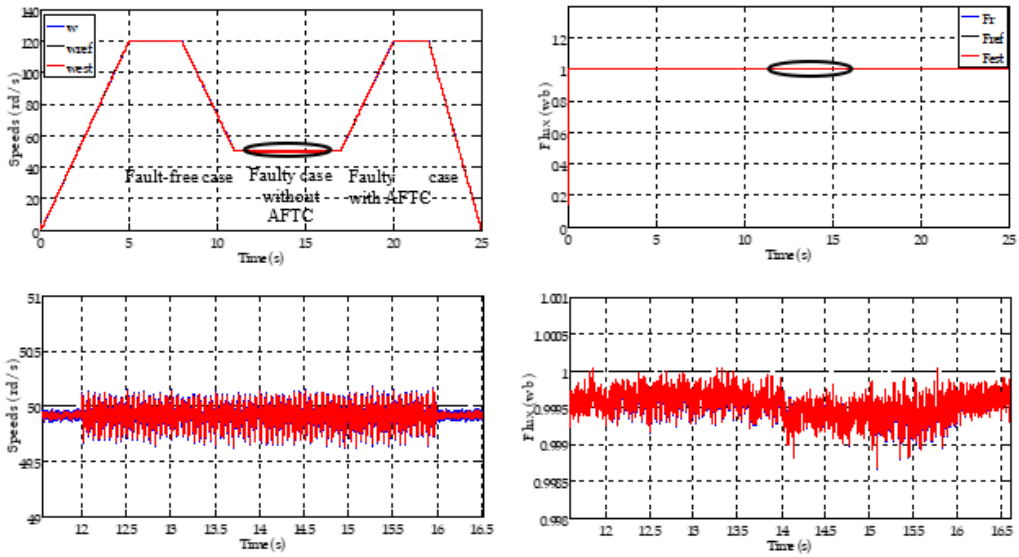

Figure 4. IMD reference, real and estimated speed and rotor flux (upper plot) with using EKF-FTC strategy, and zoom around fault appearance at t = 12 s (lower plot)

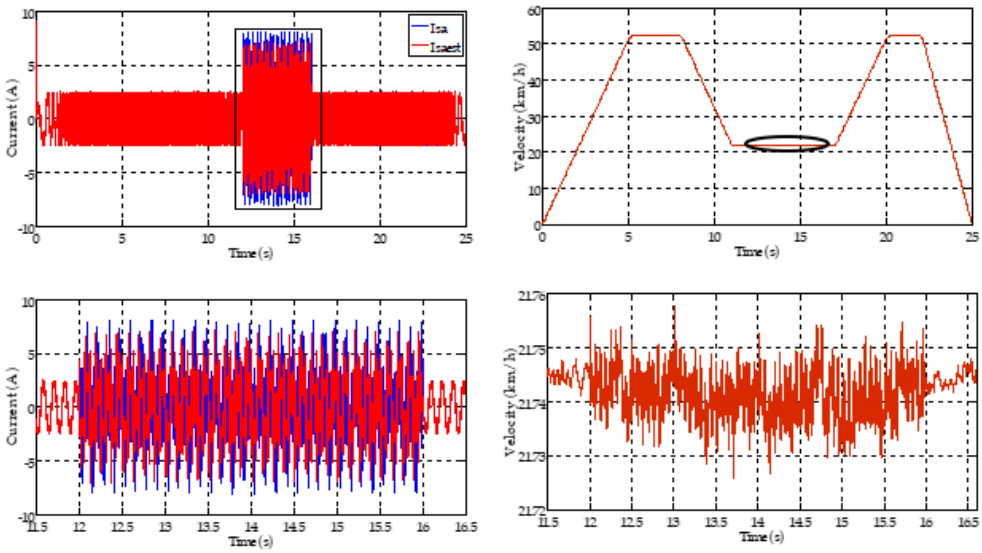

Figure 5. Current and EV velocity (upper plot) with using EKF-FTC strategy, and zoom around fault appearance at t = 12 s (lower plot)

In other words, simulation results demonstrate that the EKF is theoretically immune to external noise. In addition, EKF can provide even better performance under faulty condition, which confirms that EKF-FTC scheme shows strong robustness to faults; consequently EKF may have superior performance for fault tolerant control over LO. The results of the first strategy of FTC based on luenberger observer (LO-FTC) are presented in Figs (2) and (3).

The results of the second strategy of FTC based on extended kalman filter (EKF-FTC) are presented in Figs (4) and (5), when we used the same nominal controller (IOLC) and the same conditions applied in the previous strategy.

These results present a good performance of the input-output linearization control when we use EKF. Initially the system works on fault-free case, then at time t = 12 s, sensor faults are introduced.

From these results, we can see that the proposed control is robust to parameter variations, the preceding figures show that the use of the active FTC allows a good compensation of faults in a very short time. This is due to the use of an observer for faults reconstruction.

According these obtained results, it is noted that the nonlinear controllers with an EKF (EKF-FTC) is robust with respect to the variation of the load and the faults injection. The estimation error of speed and flux is zero for low speeds and not important for high speeds. We note from the previous figures that the method applied by the nonlinear observer allows a good reconstruction of the faults. The results obtained are more efficient than those of the active FTC used the Luenberger observer (LO-FTC).

7. CONCLUSIONS

This paper has presented a sensorless fault tolerant control with robust performance in electric vehicle based on two different observers (LO-FTC and EKF-FTC) and a nonlinear control of an induction motor drive. Novelty of the proposed fault tolerant schemes consisted of the use of the fault signal reconstructed by these observers and exploited in the closed loop scheme for improving the performances of the overall system. Further investigations will regard the proof of the stability of the complete fault tolerant scheme. Moreover, the obtained results tests proved both FTCs structures have a good response to a sudden change in the speed and parameter variations, whereas the best overall performance was recorded with the extended kalman filter.

REFERENCES

[1] Rouaibia R, Arbaoui F, Bahi T. (2017). Fault eccentricity diagnosis in variable speed induction motor drive using DWT. AMSE JOURNALS, Series: Advances C 72(3): 181-202.

[2] Gaeid K, Ping H. (2011). Wavelet fault diagnosis and tolerant of induction motor. A review. International Journal of the Physical Sciences 6(3): 358-376.

[3] Berrabah F, Chebabhi A, Zeghlache S, Saad S. (2017). Direct torque control of induction motor fed by three-level inverter using fuzzy logic. AMSE Journals, Series: Advances C 72(4): 248-265.

[4] Liu X, He R, Song Y. (2017). Clutch displacement servo control in gear-shifting process of electric vehicles based on two-speed DCT. AMSE Journals, Series: Advances C 72(2): 140-155.

[5] Yamada E, Zhao Z. (2000). Applications of electrical machine for vehicle driving system. Proceeding of Power Electronics and Motion Control Conference 3(1): 1359-1369. http://dx.doi.org/10.1109/IPEMC.2000.883051.

[6] Haddoun A, Benbouzid M, Diallo D. (2007). A loss-minimization DTC scheme for EV induction motors. IEEE Transactions on Vehicular Technology 56(1): 81-88. http://dx.doi.org/10.1109/TVT.2006.889562

[7] Kostov K, Enev S, Fnaiech F, Todorov A. (2008). Position Control of Induction Motors by Exact Feedback Linearization. Cybernetics and Information Technologies Bulgarian Academy of Sciences.

[8] Delaleau E, Louis J, Ortega R. (2001). Modeling and control of induction motors. Int. J. Appl. Math. Comput. Sci. 11(1): 105-129.

[9] Belkacem S, Naceri F, Abdessemed R. (2011). Reduction of torque ripple in DTC for induction motor using input-output feedback linearization. Serbian Journal of Electrical Engineering 8(2): 97-110. http://dx.doi.org/10.2298/SJEE1102097B

[10] Gacho J, Zalman M. (2010). IM based speed servodrive with luenberger observer. Journal of Electrical Engineering 61(3): 149-156. http://dx.doi.org/10.2478/v10187-011-0021-8

[11] Hu J, Yin D, Hori Y. (2011). Fault-tolerant traction control of electric vehicles. Control Engineering Practice 19(2): 204-213.

[12] Magallan G, Angelo C, Garcia O. (2011). Maximization of the traction forces in a 2WD electric vehicle. IEEE Transactions on Vehicular Technology 60(2): 369–380. http://dx.doi.org/10.1109/TVT.2010.2091659

[13] De Castro R, Araujo R, Freitas D. (2013). Wheel slip control of EVs based on sliding mode technique with conditional integrators. IEEE Transactions on Industrial Electronics 60(8): 3256-3271. http://dx.doi.org/10.1109/TIE.2012.2202357

[14] Nam K, Fujimoto H, Hori Y. (2014). Advanced motion control of electric vehicles based on robust lateral tire force control via active front steering. IEEE/ASME Transactions on Mechatronics 19(1): 289-299. http://dx.doi.org/10.1109/TMECH.2012.2233210

[15] Roubache T, Chaouch S, Naït-Saïd M. (2016). Backstepping design for fault detection and FTC of an induction motor drives-based Evs. AUTOMATIKA 57(3): 736-748. http://dx.doi.org/10.7305/automatika.2017.02.1733

[16] Bonivento C, et al. (2004). Implicit fault-tolerant control: Application to induction motors. Science direct. Automatica 40(3): 355-371. http://dx.doi.org/10.1016/j.automatica.2003.10.003

[17] Gu J, Ouyang M, Li J. (2010). Vehicle dynamic simulation for efficiency optimization of four-wheel independent driven electric vehicle. World Electric Vehicle Journal 4(1): 319-324.

[18] Haddoun A, et al. (2008). Modeling, analysis, and neural network control of an EV electrical differential. IEEE Trans. Industrial Electronics 55(6): 2286-2294. http://dx.doi.org/10.1109/TIE.2008.918392

[19] Roubache T, Chaouch S, Nait said M. (2014). Backstepping fault tolerant control for induction motor. Power Electronics, Electrical Drives, Automation and Motion (SPEEDAM). International Symposium, Ischia,

Italy 14(1): 472-477. http://dx.doi.org/10.1109/SPEEDAM. 2014.6871905
[20] Haddoun A, et al. (2008). comparative analysis of estimation techniques of sfoc induction motor for electric vehicles. ICEM'08, Vilamoura, Portugal, 1-6. http://dx.doi.org/10.1109/ICELMACH.2008.4800166
[21] Pacejka H, Bakker E. (1992). The magic formula tyre model. Vehicle System Dynamics 21(1): 1-18. http://dx.doi.org/10.1080/00423119208969994
[22] Metwally M. (2012). Sensorless speed and position control with dtfc of induction motor using four switch three phase inverter and adaptive flux observer. International Journal of Electrical & Computer Sciences IJECS-IJENS 12(5): 38-45.
[23] Roubache T, Chaouch S, Nait said M. (2016). Sensorless fault-tolerant control of an induction motor based electric vehicle. J Electr Eng Technol 11(5): 1423-1432. http://dx.doi.org/10.5370/JEET.2016.11.5.1423
[24] Rahme S, Meskin N. (2015). Adaptive sliding mode observer for sensor fault diagnosis of an industrial gas turbine. Control Engineering Practice 38(1): 57–74. http://dx.doi.org/10.1016/j.conengprac.2015.01.006
[25] Barut M, et al. (2008). Experimental evaluation of braided EKF for sensorless control of induction motors. IEEE Trans. Industrial Electronics 55(2): 620-632. http://dx.doi.org/10.1109/TIE.2007.911956

APPENDIX

Table 2. Induction motor parameters

1 kW, 5 Nm, Rs =1 2.75 Ω, R_r = 5.1498 Ω, Ls = 0.4991 H, L_r = 0.4331 H, L_m = 0.4331 H, J = 0.0035 kg.m